The Well and Box Types Initial Value Problems of the Defocusing mKdV Equation

Yuhan Ye(叶玉涵) and Juanjuan Wu(吴娟娟)*

College of Applied Science, Beijing Information Science and Technology University, Beijing 102206, China

(Received 22 January 2026; accepted manuscript online 27 February 2026)

We study the time evolution problems of special initial values with two discontinuities for the defocusing mKdV equation. Based on the finite-gap integral method, Whitham modulation system of the defocusing mKdV equation is derived in the form of Riemann invariants, and full-time evolution results for six types of initial values with two discontinuities are obtained in detail. The regions where rarefaction waves interact with dispersive shock waves are thoroughly analyzed. Two novel phenomena, namely soliton trains and linear wave packets, are identified and their intrinsic mechanisms are systematically illustrated. All the results are verified by numerical simulations.

DOI: 10.1088/0256-307X/43/4/040001 CSTR: 32039.14.0256-307X.43.4.040001

The discontinuous initial value problem of nonlinear evolution equations originates from the widespread discontinuous phenomena in natural and engineering fields, and it is usually used to characterize the abrupt changes in physical quantities in space or time, such as shock waves, phase transition interfaces, signal jumps, etc. The dispersive shock wave (DSW) is a prominent phenomenon arising from the time evolution of discontinuous initial values, whose two ends are respectively connected to two distinct regions (oscillatory fronts and soliton fronts), and it originates from the special waveforms generated by the interaction between nonlinearity and dispersion in the fluid motion of non-dissipative or dispersive media. DSW has been widely applied in multiple physical fields. In the field of nonlinear optics, the formation and characteristics of DSW are consistent with theoretical predictions in fiber optic experiments and space optical experiments.[1–3] In geophysics, DSW phenomena exist in the stratified environments of the ocean and atmosphere, and studies of these phenomena contribute to the in-depth understanding of geophysical processes.[4,5] In fluid dynamics, the study of DSW in viscous fluid pipelines provides a new perspective for understanding fluid flow characteristics. It has been used to explain the formation mechanism of oscillatory structures in shallow-water waves.[6,7] Through experiments and theoretical analysis, the detailed behaviors of DSW under different conditions have been identified, such as backflow and implosion phenomena arising during large-amplitude jumps.[8]

In 1965, Whitham pioneered the exploration of nonlinear dispersive waves theory[9] and proposed an averaging method to investigate the evolution of wave trains governed by nonlinear partial differential equations. This method has unique advantages in analyzing the asymptotic behavior of nonlinear dispersive waves, especially in solving the slow modulation problem of periodic wave trains in weakly nonlinear and dispersive systems. The core idea of this theory is based on the slow variation (i.e., "modulation") of wave train parameters (e.g., amplitude and wavelength) in space and time. Through the averaging process, the original partial differential equation is simplified into a set of hyperbolic equations, termed the Whitham equations, that describe the evolution of these modulation parameters. This simplification enables effective capture of large-scale wave behavior. The Whitham modulation theory is an important method for studying DSWs, and its first application was achieved by Gurevich and Pitaevskii.[10] They studied self-similar solutions of the KdV equation and described the evolution of DSWs using the diagonal form of the Whitham equations. The Riemann–Hilbert method is also an important approach for studying the evolution of nonlinear waves.[11] This method complements the Whitham modulation theory, with their results mutually corroborating each other.[12–16] Whitham modulation theory has emerged a novel and promising research direction, inspiring numerous studies.[17–20]

In this paper, we study the defocusing mKdV equation

$$u_t - 6u^2u_x + u_{xxx} = 0, \tag{1}$$

with two discontinuous initial values as follows:

$$u(x,0) = \begin{cases} a_1, & x < 0, \\ a_2, & 0 \le x \le l, \\ a_3, & x > l, \end{cases} \tag{2}$$

where a_1, a_2, a_3 are real numbers, which take the following values:

$$\text{case I } (\sqcap\!\sqcap\!\sqcap): \ a_1 > a_2 > a_3 \ge 0,$$
$$\text{case II } (\sqcap\!\sqcup\!\sqcap): \ a_1 = a_3 > a_2 \ge 0,$$
$$\text{case III } (\sqcup\!\sqcap\!\sqcup): \ a_2 > a_1 = a_3 \ge 0,$$

*Corresponding author. Email: juanjuanwu@bistu.edu.cn

© 2026 Chinese Physical Society and IOP Publishing Ltd. All rights, including for text and data mining, AI training, and similar technologies, are reserved.

case IV ( ): $a_2 < a_1 = a_3 \leq 0$,

case V ( ): $a_1 = a_3 < a_2 \leq 0$,

case VI ( ): $a_1 < a_2 < a_3 \leq 0$.

The dashed lines in the above cases denote $u = 0$. The mKdV equation is a classical model employed in numerous physics scenarios, such as the propagation of Alfvén waves in cold, collisionless plasmas and the dynamics of optical pulse propagation in optical fiber media, particularly for few-cycle pulses. Two discontinuous initial values are interpreted as potential barriers and wells in quantum mechanics,[21] serving to model the behavior of microscopic particles in a potential field. They provide an effective framework for describing quantum phenomena, including tunneling, reflection, and wave interference.[22] There have been relatively rich results on discontinuous initial value problems for the mKdV equation. Using conservation laws and the finite-gap integration method, Driscoll and Kamchatnov[23–25] independently derived the Whitham equations for the mKdV equation, laying the foundation for subsequent studies of long-time evolution behavior. Furthermore, Kamchatnov[26] studied the single-discontinuity initial value problem for the Gardner equation and discovered the kink structure. According to the signs (positive/negative) and magnitude relations of u^- and u^+, the long-time asymptotic solutions of the mKdV equation with a single discontinuous initial value can be divided into eight cases.[27] To date, comprehensive results on the two-discontinuity initial value problem for the defocusing mKdV equation remain lacking. The key findings of the present work reveal that this problem exhibits a rich variety of novel phenomena. The types of two-discontinuity initial values can be classified into three categories: step (Cases I and VI), box (Cases III and V), and well (Cases II and IV). The results of this study indicate that the step case evolves into five regions without an interaction region. In contrast, both the box and well cases undergo the overlap and interaction between the rarefaction wave (RW) and DSW regions. The major challenge of this work is to calculate the boundaries of the interaction regions by solving the Euler–Darboux–Poisson equation, transformed by Whitham modulation system of Eq. (1). Explicit or implicit expressions for the corresponding boundaries in terms of x and t are obtained. Furthermore, full-time evolution results for all six cases of two-discontinuity initial values are presented.

Case I: the Time Evolution Result of Step Initial Value. The evolution result of the step initial values divides the entire plane into five regions: plateau (I), RW (II), plateau (III), RW (IV), and plateau (V). The two RWs arise respectively from the degradation of R_1 and R_3 when the other two Riemann invariants are equal. That is, the characteristic velocity of R_1 degrades to $V_1 = -6R_1^2$ if $R_2 = R_3$, and the characteristic velocity of R_3 degrades to $V_3 = -6R_3^2$ if $R_1 = R_2$. Consequently, the front velocity of the RW controlled by R_1 is $\tau_1 = -6a_1^2$, the rear velocity τ_2 is $-6a_2^2$. Similarly, the front velocity of the RW τ_3 controlled by R_3 is $-6a_2^2$, and the rear velocity τ_4 is $-6a_3^2$. Thus, the four boundaries separating these five regions, from left to right, are given by $x_1 = \tau_1 t = -6a_1^2 t$, $x_2 = \tau_2 t = -6a_2^2 t$, $x_3 = \tau_3 t + l = -6a_2^2 t + l$, and $x_4 = \tau_4 t + l = -6a_3^2 t + l$. The evolution result for Case I ( ) is shown in Fig. 1, and the solutions in each regions are as follows: (I) $u = a_1$, $x < x_1$; (II) $u = \sqrt{-x/(6t)}$, $x_1 < x < x_2$; (III) $u = a_2$, $x_2 < x < x_3$; (IV) $u = \sqrt{-(x-l)/(6t)}$, $x_3 < x < x_4$; (V) $u = a_3$, $x > x_4$.

Case II: The Time Evolution Result of Well Initial Value. For the well-shaped initial value on the upper side of the x-axis, the initial value is

$$u(x,0) = \begin{cases} U_0, & 0 \leq x \leq l, \\ a, & \text{other}, \end{cases} \tag{3}$$

where $0 \leq U_0 < a$. It can be verified that the rear velocity of the RW τ_2 is $-6U_0^2$, and the oscillatory front velocity τ_3 is $6U_0^2 - 12a^2$, implying a chasing problem ($|\tau_2| < |\tau_3|$) between the RW (the former) and the DSW (the latter). Eventually, the interaction region expands in time and asymptotically occupies the entire perturbed region; this phenomenon is also observed in the KdV equation.[28] At the moment of collision, we can get the critical point $t_0 = l/(12a^2 - 12U_0^2)$. Therefore, the evolutionary process of the well located above the x-axis can be divided into three stages according to time, and Fig. 2(a) shows the time-evolution diagram of each boundary.

Pre-critical case: $t < t_0$. This regime occurs before the critical state, and the rear end of the RW has not yet contacted the oscillatory front. The evolution result of this initial values divides the entire plane into five regions: plateau (I), RW (II), plateau (III), DSW (Rmnum4), and plateau (V). The front velocity of the RW τ_1 is $-6a^2$, the rear velocity of the RW τ_2 is $-6U_0^2$, the oscillatory front velocity is $\tau_3 = 6U_0^2 - 12a^2$, and the

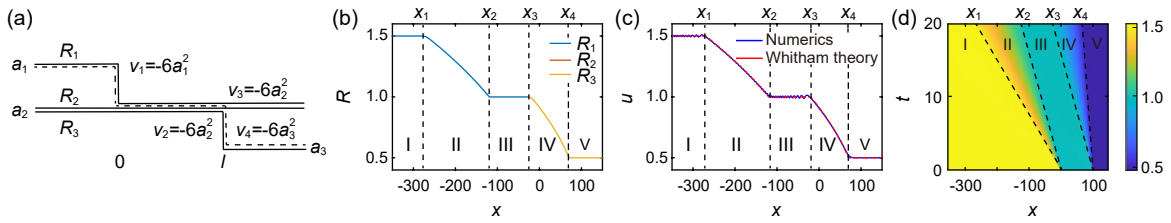

Fig. 1. Case I: The time evolution result of step initial value with $a_1 = 1.5, a_2 = 1, a_3 = 0.5, l = 100$. (a) Regularization of Riemann invariants; (b) and (c) Distribution of Riemann invariants and waveform structures of solution u at $t = 20$; (d) Density plot: the evolution of the regions of different types of solutions over time.

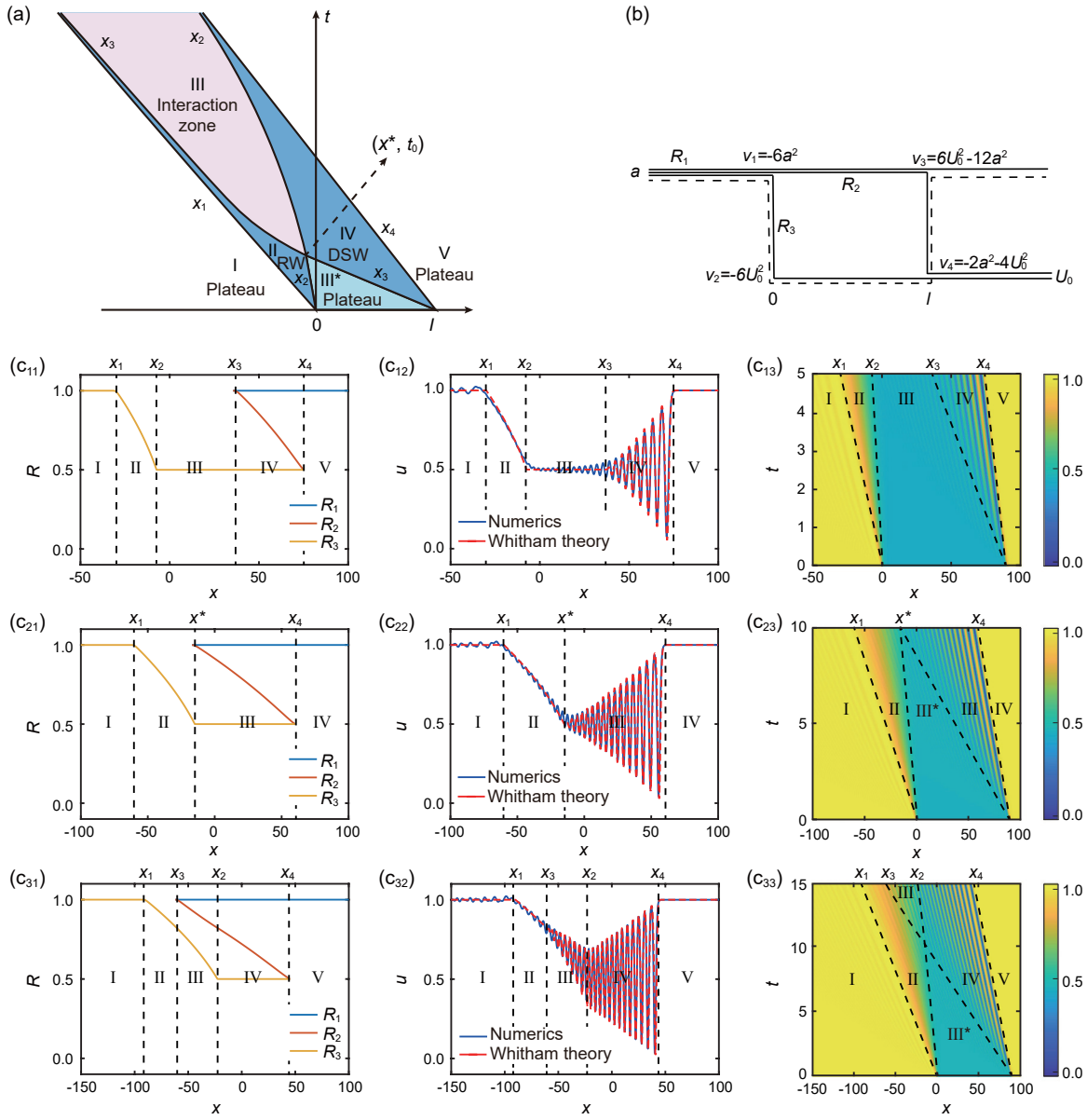

Fig. 2. Case II: The time evolution results of well initial value with $a = 1, U_0 = 0.5, l = 90$. (a) Evolution diagram of boundaries of distinct waveform region; (b) Regularization of Riemann invariants of well initial value; (c_{11})–(c_{13}) Pre-critical time case; (c_{21})–(c_{23}) Critical time case; (c_{31})–(c_{33}) Post-critical time case. (c_{i1}) and (c_{i2}) Distribution of Riemann invariants and waveform structures of solution u: $t = 5$ for $i = 1$; $t = 10$ for $i = 2$; $t = 15$ for $i = 3$; (c_{i3}) Density plot: the evolution of the regions of different types of solutions over time, where $i = 1, 2, 3$.

soliton front velocity is $\tau_4 = -2a^2 - 4U_0^2$. Combining with the initial position, the four boundaries of these five regions are: $x_1 = \tau_1 t = -6a^2 t$, $x_2 = \tau_2 t = -6U_0^2 t$, $x_3 = \tau_3 t + l = (6U_0^2 - 12a^2)t + l$, and $x_4 = \tau_4 t + l = (-2a^2 - 4U_0^2)t + l$. The result of Case II ( ) in the pre-critical regime $t < t_0$ is summarized as follows: (I) $u = a,\ x < x_1$; (II) $u = \sqrt{-x/(6t)},\ x_1 < x < x_2$; (III) $u = U_0,\ x_2 < x < x_3$; (IV) $u = u_2 + \tilde{u}(x,t),\ x_3 < x < x_4$; (V) $u = a,\ x > x_4$, where $U_1 = -2(R_1^2 + R_2^2 + R_3^2)$ and $m = (R_1^2 - R_2^2)/(R_1^2 - R_3^2)$,

$$\tilde{u}(x,t) = \frac{(u_3 - u_2)\mathrm{cn}^2[\sqrt{(u_3 - u_1)(u_4 - u_2)}(x - U_1 t - l)/2, m]}{1 - \frac{u_3 - u_2}{u_4 - u_2}\mathrm{sn}^2[\sqrt{(u_3 - u_1)(u_4 - u_2)}(x - U_1 t - l)/2, m]}.$$

See Figs. 2(c_{11})–2(c_{13}).

For the critical condition $t = t_0$, the rear end of the RW has just contacted the oscillatory front, generating a degenerate boundary $x^* = -U_0^2 l/(2a^2 - 2U_0^2)$. At this instant, the entire plane is divided into four regions: plateau (I), RW (II), DSW (III), and plateau (IV). Moreover, the result of Case II ( ) at $t = t_0$ can be expressed as follows: (I) $u = a,\ x < x_1$; (II) $u = \sqrt{-x/(6t)},\ x_1 < x < x^*$; (III) $u = u_2 + \tilde{u}(x,t),\ x^* < x < x_4$; (IV) $u = a,\ x > x_4$. Region III* denotes the plateau (III) emerging in the case

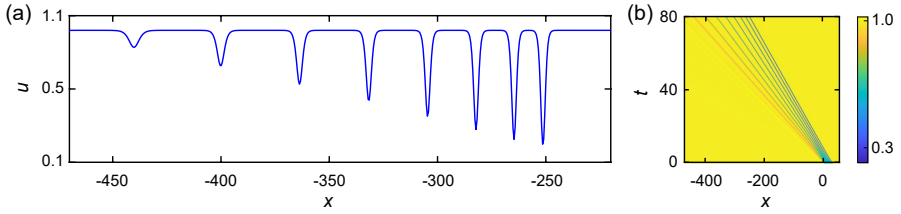

Fig. 3. Long-time evolution result of well initial value with $a = 1$, $U_0 = 0.6$, $l = 10\pi$, $t = 80$. (a) Soliton train. (b) Density plot.

of pre-critical case $t < t_0$. See Figs. 2(c$_{21}$)–2(c$_{23}$).

Post-critical case: $t > t_0$. In this regime, the rear end of the RW has interacted with the oscillatory front, triggering nonlinear collisions between the RW and DSW regions, which forms a mixed region. The evolution result of this initial values divides the entire plane into five regions: plateau (I), RW (II), mixed (III), DSW (IV), and plateau (V). The boundaries of these five regions differ significantly from those in the previous two cases. The boundary x_1 between plateau (I) and RW (II), and the boundary x_4 between DSW (IV) and plateau (V) remain unchanged. However, since the Riemann invariant R_3 is no longer constantly equal to U_0 in the mixed region, the velocity of x_3, the boundary between the RW region and mixed region, should evolve in time. Additionally, as the boundary of RW region and plateau region, the position of x_2 could be deduced from the velocity of RW before critical time. Because of nonlinear interaction of RW and DSW, x_2 becomes the boundary of mixed region and DSW region, whose velocity is determine by the velocity of DSW. The evolutionary behaviors of boundaries x_2 and x_3 can be expressed as follows:

$$x_2 = \frac{l\{1+[(U_0^2-R_2^2)(a^2-U_0^2-3R_2^2)K(m_1)-(a^2-U_0^2)(a^2+U_0^2+R_2^2)E(m_1)][(a^2-U_0^2)E(m_1)+(U_0^2-R_2^2)K(m_1)]\}}{2\sqrt{(a^2-U_0^2)(R_2^2-U_0^2)}[(U_0^2-R_2^2)K(m_1)+(a^2-U_0^2)E(m_1)][(U_0^2-R_2^2)K(m_1)+(2a^2-U_0^2-R_2^2)E(m_1)]},$$

and

$$x_3 = -6a^2t + \frac{l^2}{24(a^2-U_0^2)t},$$

where $K(m)$ and $E(m)$ are the complete elliptic integrals of the first and second kinds respectively, and $m_1 = (a^2 - R_2^2)/(a^2-U_0^2)$. The results of Case II ( ) as time evolution can be summarized as follows: (I) $u = a$, $x < x_1$; (II) $u = \sqrt{-x/(6t)}$, $x_1 < x < x_3$; (III) $u = u_2 + \tilde{u}(x,t)$, $x_3 < x < x_2$; (IV) $u = u_2 + \tilde{u}(x,t)$, $x_2 < x < x_4$; (V) $u = a$, $x_4 < x$. See Figs. 2(c$_{31}$)–2(c$_{33}$).

In particular, for the case where the well is located above the x-axis, when t is large enough, the RW and DSW regions have almost evolved adequately, and a soliton train emerges within the mixed region, as shown in Fig. 3. The mechanism of generation of soliton train is the interaction between the RW and oscillatory front. For long-time evolution, the DSW not only catches up with the RW but also undergoes complete interaction. The disperssive and nonlinear effects of DSW tend to balance in the interaction region as $t \to +\infty$, leading to the formation of a soliton train. The distance between solitons in the soliton train increases with time, whereas their amplitudes do not change. The number of solitons in the soliton train is determined by [29]

$$N \approx \frac{1}{\pi}\int_{-\infty}^{+\infty}\sqrt{a^2-u^2(x,0)}\,\mathrm{d}x. \tag{4}$$

From Eq. (4), the number of solitons is independent of time. However, with the extension of the interaction region, the distance of each soliton in soliton train increases. As shown in Fig. 3, with $a = 1$, $U_0 = 0.6$, $l = 10\pi$ in Eq. (4), there are eight solitons in soliton train, which is consistent with the numerical simulation results.

Case III: The Time Evolution Result of Box Initial Value. For the box-shaped initial value on the upper side of the x-axis, the initial value is given by Eq. (3), where $0 \le a < U_0$. Compared with the well-shaped initial value, it should be noted that the front speed of the soliton τ_2 is $-2U_0^2 - 4a^2$, and the front speed of the RW τ_3 is $-6U_0^2$. It is converted into the chasing problem of RW after DSW ($|\tau_2| < |\tau_3|$). The front edge of the RW catches up with the soliton front of DSW, but never approaches the oscillatory front of DSW. As time evolves, the DSW region, the RW region, and their interaction region all expand. However, the interaction region is confined within the "linear wave packet", and does not fill the entire perturbed domain. At the moment of collision, the critical point is $t_0 = l/(4U_0^2 - 4a^2)$. Therefore, the evolutionary process of the box on the upper side of the x-axis can be divided into three stages according to time, and Fig. 4(a) shows the time-evolution diagram of each boundary.

Pre-critical case: $t < t_0$. For this case, the front of the RW has not yet contacted the soliton front. During this time interval, the entire plane is divided into five regions by different evolutionary waveforms: plateau (I), DSW (II), plateau (III), RW (IV), and plateau (V). The velocity of the oscillatory front τ_1 is $6a^2 - 12U_0^2$, the front velocity of the soliton τ_2 is $-2U_0^2 - 4a^2$, the front velocity of the RW τ_3 is $-6U_0^2$, and the rear velocity of the RW τ_4 is $-6a^2$. Combining with the initial positions, the four boundaries separating these regions are: $x_1 = (6a^2 - 12U_0^2)t$, $x_2 = (-2U_0^2 - 4a^2)t$, $x_3 = -6U_0^2t + l$, $x_4 = -6a^2t + l$. In summary, the solution for Case III ( ) as time evolution when $t < t_0$ is: (I) $u = a$, $x < x_1$; (II) $u = u_2 + \tilde{u}(x + l, t)$, $x_1 < x < x_2$; (III) $u = U_0$, $x_2 < x < x_3$; (IV) $u = \sqrt{-(x-l)/(6t)}$, $x_3 < x < x_4$; (V) $u = a$, $x > x_4$. See Figs. 4(c$_{11}$)–4(c$_{13}$).

Critical time: $t = t_0$. The time $T = t_0$ at which the front of the RW just contacts the front of the soliton,

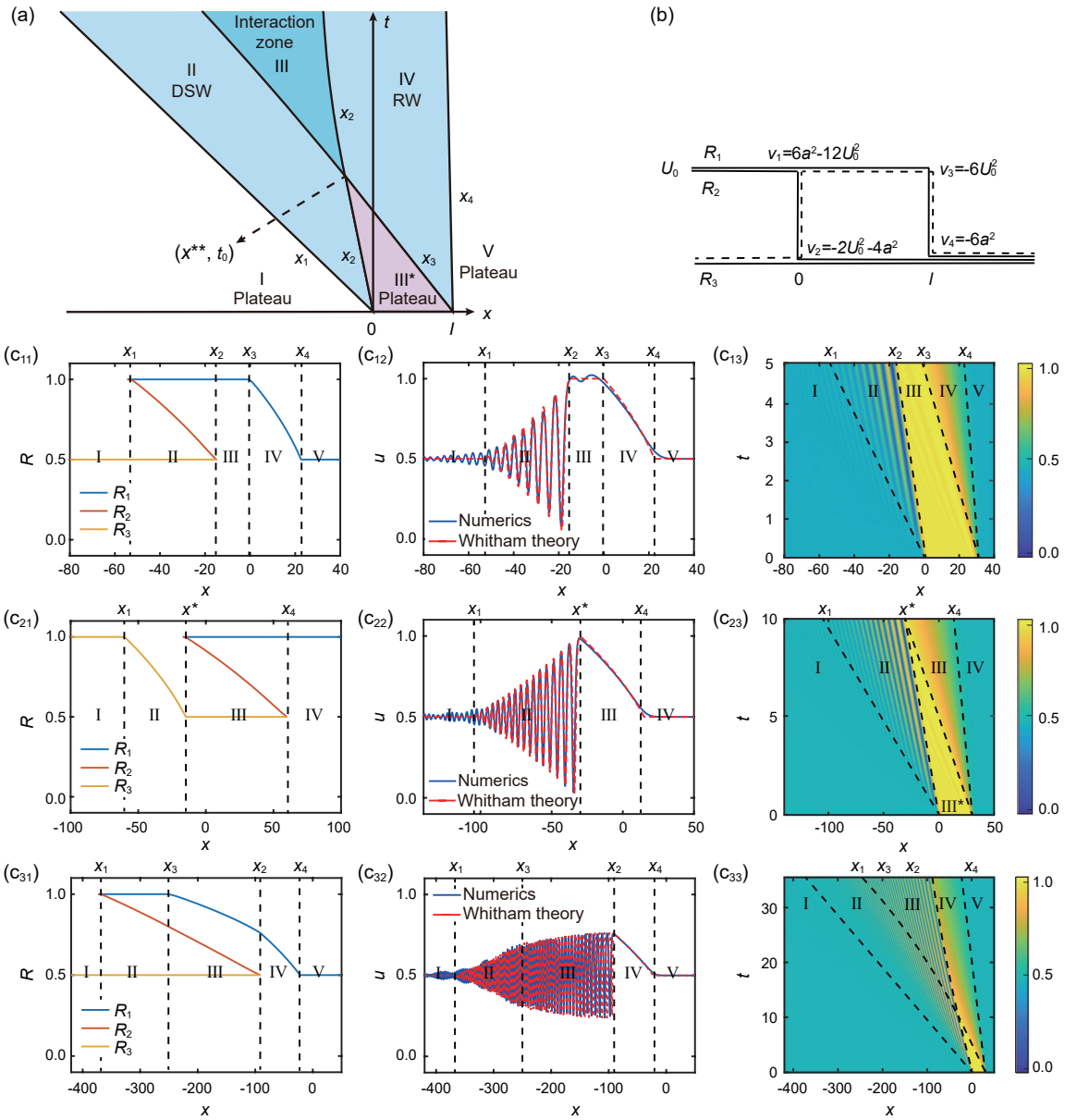

Fig. 4. Case III: The time evolution results of box initial value with $a = 0.5$, $U_0 = 1$, and $l = 30$. (a) Evolution diagram of boundaries of distinct waveform region; (b) Regularization of Riemann invariants of box initial value; (c_{11})–(c_{13}) Pre-critical time case; (c_{21})–(c_{23}) Critical time case, $t = 10$; (c_{31})–(c_{33}) Post-critical time case; (c_{i1}) Distribution of Riemann invariants; (c_{i2}) Waveform structures of solution u; (c_{i3}) Density plot: the evolution of the regions of different types of solutions over time, where $i = 1, 2, 3$.

causing the original region III to vanish, is termed the critical time. At this instant, the entire plane is divided into four regions by evolutionary waveforms: plateau (I), DSW (II), RW (III), and plateau (IV). Due to the absence of plateau (III) in case $t < t_0$, the left edge x_2 and the right edge x_3 degenerate into $x^{**} = -(U_0^2 + 2a^2)l/(2U_0^2 - 2a^2)$. The result of Case III ( ) as time evolution at $t = t_0$ is summarized as follows: (I) $u = a$, $x < x_1$; (II) $u = u_2 + \tilde{u}(x+l, t)$, $x_1 < x < x^{**}$; (III) $u = \sqrt{-(x-l)/(6t)}$, $x^{**} < x < x_4$; (IV) $u = a$, $x > x_4$. Region III* denotes plateau (III) emerging in the case of pre-critical case $t < t_0$. See Figs. 4(c_{21})–4(c_{23}).

Post-critical case: $t > t_0$. Similar to the well case in the upper half-plane of the x-axis, there exists an interaction region caused by RW and DSW when $t > t_0$. In this time interval, the entire plane is divided into five regions by evolutionary waveforms: plateau (I), DSW (II), mixed (III), RW (IV), and plateau (V). The evolutionary behaviors of boundaries x_2 and x_3 can be represented as follows:

$$x_2 = -6a^2 t - \frac{3}{2} l^{\frac{2}{3}} [4(U_0^2 - a^2)]^{\frac{1}{3}} t^{\frac{1}{3}} + l,$$

and

$$x_3 = -\frac{l[(U_0^2 - a^2)E(m_2) + (a^2 - R_2^2)K(m_2)][(a^2 - U_0^2)(a^2 + U_0^2 + R_2^2)E(m_2) - (a^2 - R_2^2)(a^2 - U_0^2 + 3R_2^2)K(m_2)]}{2\sqrt{(U_0^2 - a^2)(U_0^2 - R_2^2)[(U_0^2 + R_2^2 - 2a^2)E(m_2) + (2a^2 - 2R_2^2)K(m_2)][(R_2^2 - a^2)K(m_2) + (a^2 - U_0^2)E(m_2)]}},$$

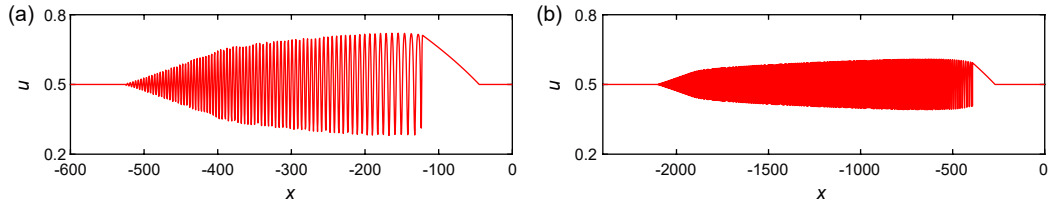

Fig. 5. The generation process of linear wave packet with $a = 0.5$, $U_0 = 1$, $l = 30$. (a) $t = 50$; (b) $t = 200$.

Table 1. Full-time evolution results for all the six cases of initial values with two discontinuities.

Case	I	II	III	IV	V	VI
$t < t_0$						
$t = t_0$						
$t > t_0$						

where $m_2 = (U_0^2 - R_2^2)/(U_0^2 - a^2)$. In summary, the result of Case III ( ) as time evolution when $t > t_0$ is: (I) $u = a,\ x < x_1$; (II) $u = u_2 + \tilde{u}(x+l,t),\ x_1 < x < x_3$; (III) $u = u_2 + \tilde{u}(x+l,t),\ x_3 < x < x_2$; (IV) $u = \sqrt{-(x-l)/(6t)}$, $x_2 < x < x_4$; (V) $u = a,\ x > x_4$. See Figs. 4(c$_{31}$)–4(c$_{33}$).

For the soliton front, the amplitude of the soliton is

$$A = 2\left(\sqrt{a^2 + \frac{1}{4}l^{\frac{2}{3}}[4(U_0^2 - a^2)]^{\frac{1}{3}}t^{-\frac{2}{3}}} - a\right).$$

It can be seen that, as time increases, the soliton amplitude gradually decreases and eventually tends to zero. Physically, it can be attributed that, when the RW catches up with the soliton front, an interaction region between the RW and the DSW emerges, the characteristic properties of the RW restrains the soliton amplitude to decrease gradually. However, since the velocity of the RW front is slower than that of the oscillatory front, the oscillatory front continuously generates solitons, which are trapped within the "linear wave packet", as shown in Fig. 5 at different times.

The remaining three cases, Case IV, Case V, and Case VI, whose discontinuous initial values are located in the lower half-plane of the x-axis, can be derived analogously by exploiting the symmetry of u with respect to the x-axis, as shown in Table 1.

Acknowledgements. This work was supported by the National Natural Science Foundation of China (Grant No. 12301305).

References

[1] Wan W, Jia S, and Fleischer J W 2007 *Phys. Rev. Lett.* **99** 223901
[2] Wang J L, Wen W, Lin J, and Li H J 2023 *Chin. Phys. Lett.* **40** 070302
[3] Belyaeva T L and Serkin V N 2024 *Chin. Phys. Lett.* **41** 080501
[4] Smyth N F and Holloway P E 1988 *J. Phys. Oceanogr.* **18** 947
[5] Apel J R 2002 *An Atlas of Internal Solitary-like Waves and their Properties* **1** 1
[6] Trillo S, Klein M, Clauss G F, and Onorato M 2016 *Physica D: Nonlinear Phenomena* **333** 276
[7] Yang Z, Zhong W P, and Belić M 2024 *Chin. Phys. Lett.* **41** 044201
[8] Lowman N K and Hoefer M A 2013 *J. Fluid Mech.* **718** 524
[9] Whitham G B 1965 *Proc. R. Soc. Lond. A* **283** 238
[10] Gurevich A V and Pitayevsky L P 1974 *Sov. J. Exp. Theor. Phys.* **38** 291
[11] Yang J J, Tian S F, and Li Z Q 2026 *Adv. Math.* **484** 110552
[12] Gong R and Wang D S 2022 *Appl. Math. Lett.* **126** 107795
[13] Gong R and Wang D S 2023 *Acta Phys. Sin.* **72** 100503 (in Chinese)
[14] Wang D S and Yan P 2025 *Nonlinearity* **38** 125006
[15] Wang D S and Wen D 2026 *J. Differ. Equ.* **454** 113952
[16] Wu Z J and Tian S F 2024 *Stud. Appl. Math.* **153** e12779
[17] El G A and Hoefer M A 2016 *Physica D: Nonlinear Phenomena* **333** 11
[18] Gurevich A V, Krylov A L, and El G A 1992 *Zh. Eksp. Teor. Fiz* **101** 1797
[19] Gurevich A V and Krylov A L 1987 *Zh. Eksp. Teor. Fiz* **92** 1684
[20] Ablowitz M J, Biondini G, and Wang Q 2017 *Proc. R. Soc. A* **473** 20160695
[21] Cheng F and He B 2016 *Chin. Phys. Lett.* **33** 057301
[22] Li C F and Wang Q 2000 *Chin. Phys. Lett.* **17** 902
[23] Driscoll C F and O'Neil T M 1976 *J. Math. Phys.* **17** 1196
[24] Kamchatnov A M 2000 *Nonlinear periodic waves and their modulations: an introductory course* (Cambridge: World Scientific)
[25] Kamchatnov A M, Spire A, and Konotop V V 2004 *J. Phys. A: Math. Gen.* **37** 5547
[26] Kamchatnov A M, Kuo Y H, Lin T C, Horng T L, Gou S C, Clift R, El G A, and Grimshaw R 2012 *Phys. Rev. E* **86** 036605
[27] de Brito L F C and Kamchatnov A M 2024 *Phys. Rev. E* **109** 015102
[28] El G A and Grimshaw R H J 2002 *Chaos* **12** 1015
[29] Karpman V I 1967 *Phys. Lett. A* **25** 708